Engineered Heterostructures of 6.1 Å III-V Semiconductors for Advanced Electronic and Optoelectronic Applications

B. V. Shanabrook, W. Barvosa-Carter, R. Bass, B. R. Bennett, J. B. Boos, W. W. Bewley, A. S. Bracker, J. C. Culbertson, E. R. Glaser, W. Kruppa, R. Magno, W. J. Moore, J. R. Meyer, B. Z. Nosho, D. Park, P. M. Thibado, M. E. Twigg, R. J. Wagner, J. R. Waterman, L. J. Whitman and M. J. Yang
Naval Research Laboratory, Washington, DC 20375-5000

Keywords: High-speed electronics, IR lasers, IR detectors, band structure engineering, epitaxy, InAs, GaSb, AlSb

ABSTRACT

Heterostructures formed from III-V semiconductors with the 6.1 Å lattice spacing (InAs, GaSb, AlSb and related alloys) have attracted significant interest because of their potential to define a new 'state of the art' in applications including 100 GHz high-speed logic circuits, terahertz transistors, sensitive infrared detectors and mid-infrared semiconductor lasers. In this paper, we describe the ongoing work at the Naval Research Laboratory to develop the materials growth and fabrication technology for a variety of 6.1 Å-based devices that have the potential to revolutionize infrared optoelectronics and low-power, high-speed electronics.

1. INTRODUCTION

The nearly lattice-matched 6.1 Å III-V semiconductor material system (InAs/GaSb/AlSb) provides enormous flexibility in designing novel electronic and optical devices. Specifically, long-wave infrared (IR) detectors,[1] mid-wave IR lasers,[2] high-frequency field effect transistors[3] (FETs) and resonant interband tunneling diodes[4] (RITDs) have been demonstrated. However, many of these applications require control of structural and electronic properties with individual layer thicknesses of several nanometers. Quantum heterostructures with such narrow layers provide significant challenges to MBE growth technology, conventional materials characterization techniques, heterostructure physics simulations and device modeling. The issues being addressed at the Naval Research Laboratory include: the development of methods to manipulate structure on the nanometer length scale and thereby better control epitaxial growth, the implementation of new characterization techniques with the capability to measure structural imperfections on the nanometer length scale, and a determination of the impact of structural imperfections on device performance and property simulation. In addition to these fundamental studies, we have ongoing device programs aimed at developing high-speed, low-power electronics, mid-wave IR lasers and long-wave IR detectors. In this review we describe both the materials characterization efforts and device programs.

The advanced heterostructures discussed in this review were grown in the *Epicenter for Advanced Materials Growth and Characterization* at the Naval Research Laboratory. This facility consists of four, interconnected ultrahigh vacuum systems for molecular beam epitaxy (MBE) film growth and film analysis. One system is dedicated to the growth of II-VI semiconductors and magnetic metals for the development of magnetoelectronic devices. In the other MBE machine, III-V compounds are grown, with a special focus on InAs, GaSb, and AlSb-based heterostructures. The angle resolved electron spectrometer and the scanning tunneling microscope (STM) are housed in the two other ultrahigh vacuum systems. *In situ* film analysis is accomplished with reflection

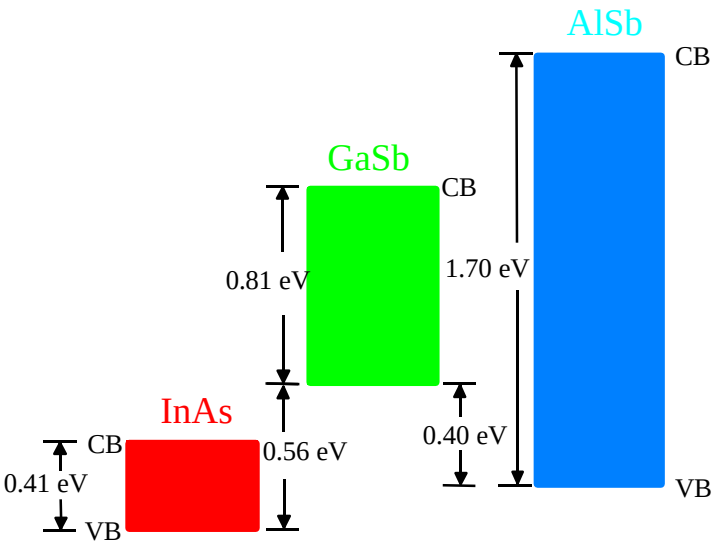

Figure 1—The relative energy alignments of the conduction band (CB) and valence band (VB) edges of InAs, GaSb and AlSb at 0K. The forbidden energy gaps are given by the colored rectangles.

high-energy electron diffraction (RHEED), optical absorption measurements, angle-resolved electron spectroscopy and scanning tunneling microscopy (STM). These techniques provide information about the growth temperature, growth rate, elemental composition, bonding configurations, and morphology of the MBE-grown films.

The diversity of applications offered by the 6.1 Å III-V material system arises from the relative band alignments of the different heterostructures and the resulting flexibility in band structure engineering. Shown in Figure 1 are the bandgaps and relative band alignments between InAs, GaSb and AlSb. Many of the novel properties exhibited by this heterostructure system are a consequence of the relative band alignments between InAs and GaSb. Because the conduction band of InAs is lower that the valence band of GaSb, one has the ability to tune the band gap of heterostructures from practically zero to ~1 eV.

2. MATERIAL CHARACTERIZATION

Because of the narrow layer thicknesses (~30 Å) required for many of the novel device structures in the 6.1 Å family, it is important to minimize interface imperfections. These imperfections cause carrier localization (i.e. lower mobilities), lead to violations in wavevector conservation rules (decrease in Auger lifetimes and peak-to-valley ratios in RITDs) and broaden optical linewidths (poor laser efficiencies). Furthermore, there is a growing wealth of experimental information obtained from high-resolution transmission electron microscopy (HRTEM), STM, Raman scattering and photoluminescence (PL) which suggest that the power spectrum that characterizes interface disorder is bimodal. Interfacial roughness and intermixing are two classes of interfacial disorder that lead to the bimodal distribution.[5] Monolayer (ML) variations in the structure of the interface caused by islands and vacancy islands that form on the growing surface due to kinetic and thermodynamic effects characterize the first class. The second arises from diffusion or exchange reactions that occur between the different elements during or after the formation of the interface. Significant progress has been made in the last several years that allow these classes of interface roughness to be modified individually by changing growth techniques. For example, interruption of the growth process allows the atoms to migrate on the surface and form large islands and thereby tune the interface roughness. By careful control of the anion flux, interrupt time and substrate temperature, the size of the islands can be controlled, and in some cases, be allowed to grow to sizes that approach 0.5 μm in lateral extent. In addition, the degree of intermixing at the interface can be modified by different growth procedures and by changing the temperature of the substrate during the growth of the interface.

Although the 6.1 Å materials offer engineering possibilities that do not exist in the well-studied GaAs/AlGaAs system, the MBE growth processes are more complex. Specifically, heterostructures formed from binary semiconductors with constituent layers that do not contain either a common anion or cation offer new flexibility in materials engineering that is only beginning to be explored from experimental and theoretical viewpoints. This flexibility arises because heterojunctions formed between AB and CD semiconductors can be bonded by either AD or BC bonds. An illustration of a particular bond type is shown schematically in Figure 2. Different interface bond types have been shown to have a significant impact on heterojunction band alignments, band structure and carrier mobility. Because these fundamental material properties determine the performance of any device, it is important to develop growth techniques and procedures that allow interfacial bonding geometry to be controlled and tuned to best advantage. Unfortunately, the results obtained from many of the commonly employed experimental techniques used for materials characterization, such as luminescence, absorption, and transport, are difficult to relate to interface bonding geometry. This illustrates the need to develop experimental techniques that are sensitive to structure at the monolayer level. These ongoing developments aid in understanding the fundamental issues of growth at the atomic scale and allow the achievement of flexible and controlled growth of the technologically important GaSb/InAs and AlSb/InAs interfaces.

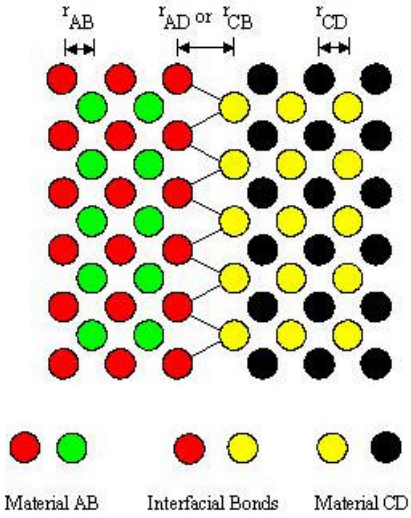

Figure 2—Schematic illustration of interfacial bonds that can be formed in heterostructures with neither common cation nor anion.

Through the application of migration-enhanced epitaxy, we have developed methods of controlling the intermixing at the GaSb/InAs[6] and AlSb/InAs[7] interfaces. This knowledge base was reached via a coordinated interdisciplinary program that combined the results of MBE growth, x-ray diffraction, Raman scattering[8], PL, STM[9] and HRTEM[10]. Although we have concluded that the chemical composition of the interface can be controlled, interface roughness is still present at the interfaces between materials. Using the STM capability in the Epicenter at NRL, we can study the topography of the surface

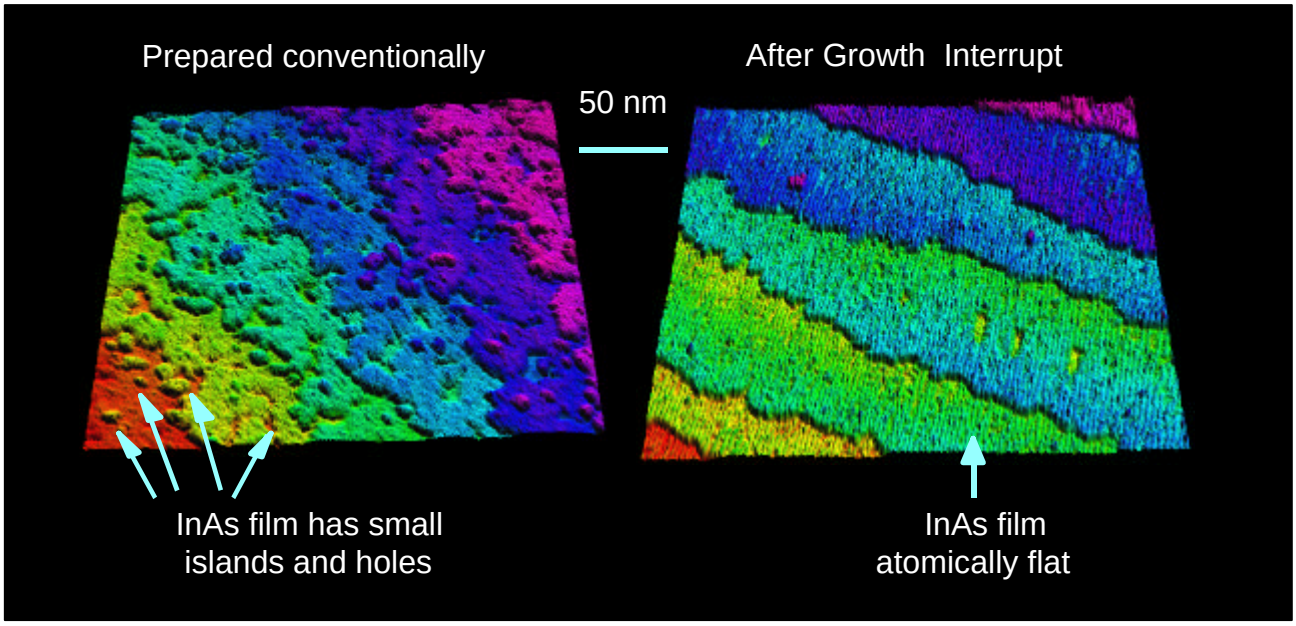

Figure 3—Plan-view STM image of an InAs surface prepared conventionally and after a growth interrupt of several minutes. Each change of color corresponds to a change in height of 1 ML (0.3 nm).

under a variety of growth conditions and determine their influence on interface roughness. Our earliest STM studies focused on the topography of surfaces during the growth of short period InAs/GaSb superlattices as a function of interface type (i.e. GaAs-like or InSb-like). We found that the interfaces on GaSb are smoother than those on strained InAs, and that the InSb-like interfaces are smoother that the GaAs-like ones. In agreement with our HRTEM measurements, the primary source of disorder at these interfaces appears to be interface roughness. This roughness occurs as a consequence of the kinetically-determined topography of the growth surface. Therefore, the surface topography can be made smoother by growth interrupts, and we can control the island size and thereby, interface roughness.

The research at NRL illustrates clearly that interface roughness and intermixing are two classes of interfacial disorder that need to be better controlled. Shown in Figure 3 is a plan-view STM images of 8 MLs of InAs on GaSb obtained during the growth of an InAs/GaSb superlattice. The conventionally grown surface is characterized by monolayer variations (0.3 nm) in the topography of the surface caused by islands and vacancy islands that form during growth because of kinetic and thermodynamic effects. In this case, performing a growth interrupt that allows for the migration of cations to sites of lower energy can reduce the concentration of islands and pits. This is a complex process that depends on temperature and the magnitude of biaxial strain experienced by the layers. If the strain is too large the low energy surface is no longer flat and surface undulations or quantum dots can form during the growth interrupt. In addition, growth interrupts result in an increase in the time required to grow the structure and can result in the inadvertent introduction of impurities at the interface.

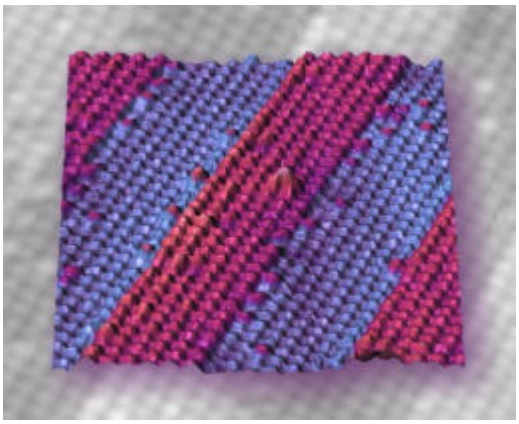

Figure 4—A color-enhanced 3D cross-sectional STM image of a GaSb/InAs superlattice performed on a cleaved (110) surface. The Sb (red) and As (blue) atoms can be seen.

While plan-view STM and RHEED allow growth procedures to be developed that result in flat surfaces, other techniques are required that are sensitive to segregation, diffusion and exchange reactions that occur between the different elements during the formation of the interface. We have employed cross-sectional STM, HRTEM, x-ray diffraction and Raman scattering to determine the magnitude of interfacial intermixing as a function of the MBE substrate temperature and the molecular beam fluxes employed during the formation of the interface. Shown in Figure 4 is an illustration of the information that can be obtained from cross-sectional STM. This color-enhanced 3-D rendered STM image shows the

atomic-scale structure of the interfaces between GaSb and InAs in cross-section. A superlattice of alternating GaSb (12 MLs) and InAs (14 MLs) was grown by MBE. A piece of the wafer was cleaved in vacuum to expose the (110) surface, and then the tip was positioned over the superlattice about 1 µm from the edge. Due to the structure of the crystal, only every-other lattice plane is exposed on the (110) surface, where only the Sb (red) and As (blue) atoms can be seen. The atoms are 4.3 Å apart along the rows, with a corrugation of <0.5 Å. From this image, one can clearly observe the excellent control achieved in the growth process as well as the power of the STM technique. Specifically, a careful examination of the InAs layers (blue layers) reveals that a small number of Sb atoms (red peaks) have segregated into the InAs layers.

Using a combination of the above-mentioned techniques, we are able to determine and modify the amount of interface roughness and intermixing present in resonant tunneling structures.[11] Furthermore, we are able to determine how each of the interfaces in the structure differ. Armed with this information, device structures are grown and their performance measured. Because of the close interaction between the material scientists, physicists, chemists and electrical engineers, we are able to iteratively design and optimize sample structures and determine the relationship between changes in material properties with the resulting device characteristics.

3. HIGH-SPEED ELECTRONIC DEVICES

The material properties that have the greatest impact on the high-speed performance of high electron mobility transistors (HEMTs) are the sheet charge density in the two-dimensional electron gas and the effective electron velocity. In recent years, this has led to the use of $In_xGa_{1-x}As$ channel HEMTs with increasing mole fractions of InAs. For relatively small values of x (< 0.2), GaAs substrates are suitable. For x values near 0.5, InP substrates are nearly lattice matched to the $In_xGa_{1-x}As$. This class of FETs is commonly referred to as InP-based HEMTs. For higher InAs mole fractions, however, lattice mismatch becomes a problem. For this reason, we are investigating HEMTs with InAs channels and AlSb barriers (lattice mismatch = 1.3%).[12] Shown in Figure 5 is a simplified energy level diagram from this heterostructure. The width of the InAs layer is typically ~100 Å. Advantages of this material system include the high electron mobility (30,000 cm^2/V-s) and velocity (4 x 10^7 cm/s) of InAs, and a large conduction band offset between InAs and AlSb (1.35 eV). As a consequence of these excellent intrinsic properties, single quantum wells of InAs clad by AlSb are predicted to define a new state of the art in low-power, high-frequency HEMTs.

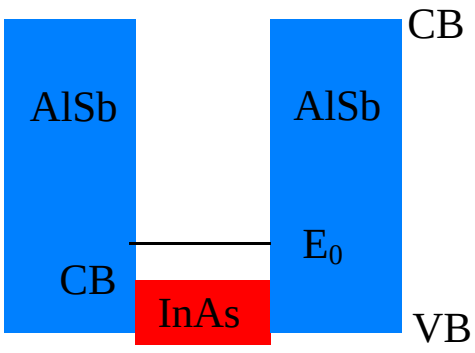

Figure 5—Energy level diagram for a HEMT composed from InAs and AlSb. E_0 is the energy of the lowest conduction subband.

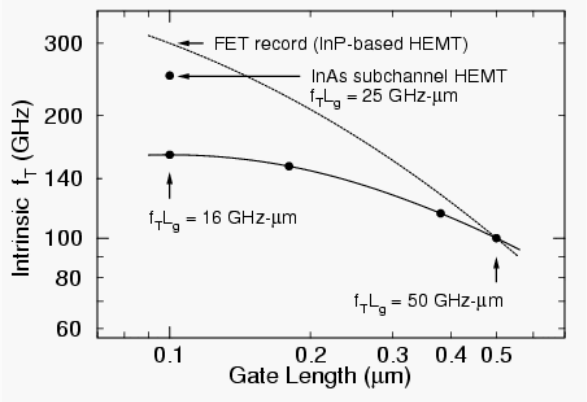

Figure 6—A comparison between the high-speed performance of InP-based and InAs/AlSb-based HEMTs as a function of gate length.

In order to achieve higher performance in the InAs FETs, a higher electron channel density is required. While Si is used as the conventional n-type dopant in GaAs, AlGaAs and InAs, Si-doping in AlSb and GaSb produces p-type conductivity. Therefore, Si doping of the AlSb can not be employed for modulation doping in AlSb/InAs FETs. In order to achieve the higher electron density a novel method was designed to increase the electron channel density through the use of a 4 ML Si-doped InAs quantum well.[13] Because of the large confinement energy of such a narrow quantum well and because Si-doping in InAs results in n-type conductivity, the electrons from the n-doped InAs layer transfer to the 50 ML wide InAs channel. The challenge in this approach was to develop a procedure to keep the Si atoms from segregating into the AlSb and causing self-compensation of the Si-donors in the InAs by Si-acceptors in the AlSb. Hall effect measurements on narrow Si-doped

InAs quantum wells were employed to determine the feasibility of the proposed approach under a variety of growth conditions. At the normal growth temperature of 500 °C more than 50% of the Si atoms segregate out of the 4 ML-wide InAs layer and n-type conductivity is not obtained. However, by lowering the growth temperature to 400 °C during the growth of the 4 ML wide InAs well, n-type conductivity was achieved. When the 4 ML n-doped InAs well was employed as a source for the modulation doping of the channel, densities as high as 3.2 x 10^{12} cm^{-2} were obtained.

A comparison between the current gain cutoff frequency (f_T) of InP-based and InAs/AlSb-based HEMTs as a function of gate length (L_g) is shown in Figure 6. Both technologies exhibit record setting $f_T L_g$ products at L_g =0.5 μm. At the shorter gate lengths, the performance of the InAs/AlSb HEMTs do not scale as well as the InP-based HEMTs. Impact ionization in the channel and the resulting loss in charge control causes degradation in performance at the shorter gate lengths. In order to lower the effects of impact ionization, HEMTs with a 0.1 μm gate length have been fabricated with the new modulation doping technique and with a thin InAs subchannel separated from the InAs channel by 30 Å of AlSb.[14] The InAs subchannel was employed to reduce impact ionization in the channel. This new HEMT design exhibited improved charge control and a higher current gain cutoff frequency. These devices exhibit a microwave transconductance of 850 mS/mm and an f_T of 180 GHz at a drain/source voltage (V_{DS}) of 0.6 V. After subtracting the gate bonding pad capacitance, an intrinsic f_T of 250 GHz was estimated. As indicated in Figure 6, these results define a world record for this materials system and are approaching the current f_T performance record for L_g =100 nm held by InP-based HEMTs. We anticipate that the optimization of the subchannel design will allow us to fully exploit the reduction of impact ionization and allow the InAs/AlSb-based FETs to exhibit the highest f_T of any technology. As indicated in Figure 7, this research also demonstrates the excellent high-frequency performance of InAs/AlSb FETs at low drain voltages.[15] This performance at low drain voltages is better than any other HEMT technology and indicates the significant advantages that InAs/AlSb HEMTs exhibit in the low-power, high frequency application arena.

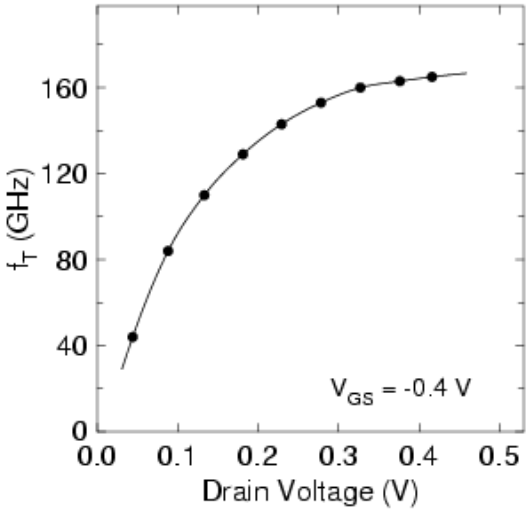

Figure 7—Illustration of the high frequency performance of InAs/AlSb HEMTs with L_g=60 nm at low drain voltages.

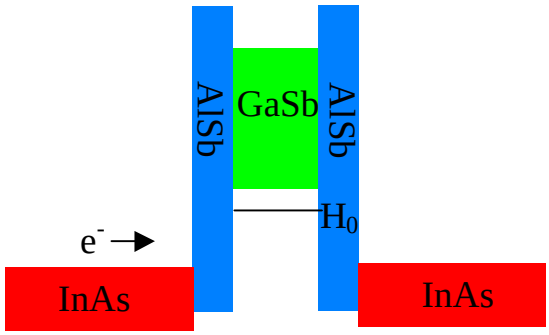

Figure 8—Energy level diagram of a resonant interband tunneling diode. In this structure the electrons, e^-, from the conduction band of InAs tunnel into the H_0 valence subband of the GaSb.

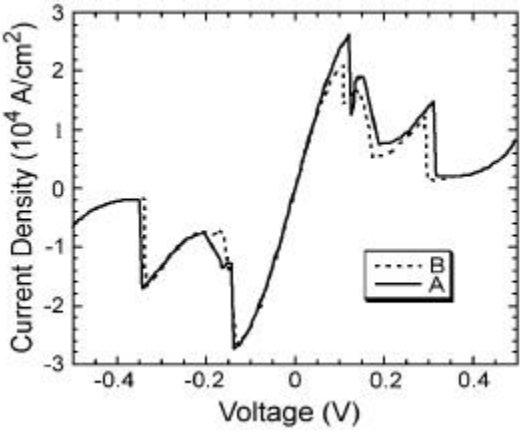

Figure 9—Current density verses voltage for a RITD of the type shown in Figure 8. Curves A and B resulted from changes in interface structure discussed in reference 17.

Resonant tunneling diodes (RTDs) made using InAs, GaSb, and AlSb have been shown to operate at frequencies as high as 712 GHz.[16] Therefore these materials could serve as components in digital circuits operating at frequencies orders of magnitude faster than those available today. To obtain devices operating at these high frequencies it is necessary to produce

RTDs with peak currents >10^4 A/cm^2 and high peak to valley ratios. The peak current requirement means that the tunnel barriers must be 4 to 5 MLs thick. Resonant interband tunneling diodes (RITDs) with large peak-to-valley ratios are obtained from the heterostructure design shown in Figure 8. In this design, electrons in the InAs layer tunnel through the AlSb barrier into the valence band of the GaSb. This structure exhibits a small valley current because beyond the resonance, electrons must tunnel through the forbidden gap of the GaSb. The small magnitude of the staggered band offset results in a low peak voltage. Shown in Figure 9 is a plot of the current density obtained from the design shown in Figure 8 with 5 ML (15 Å) AlSb barriers and 27 ML (82 Å) GaSb wells.[17] This device exhibits a peak current density of 2.6 x 10^4 A/cm^2 and a peak to valley ratio of ~15. These devices can operate at low powers because the peak current occurs at voltages of only ~100 mV.

In order to obtain the largest peak-to-valley ratio it is important to eliminate the nonresonant transport mechanisms caused by structural imperfections. These imperfections can cause a breakdown of wavevector conservation in the tunneling process and result in an increase in the valley current. An effort is underway at NRL to understand the electron transport in the RITD, and how it is related to the structure of the interfaces between the different semiconductors. Interface roughness scattering, impurity scattering and electron-phonon scattering at the interfaces and in the RITD layers need to be understood to optimize performance. The close interaction between the scientists performing MBE growth and the diverse characterization techniques has allowed for the growth of high quality 6.1 Å RITDs. This collaboration has provided fundamental insight into the impact of different growth procedures and surface reconstructions on interface formation. This detailed understanding of interface structure is being related to device performance.

Logic circuits composed of antimonide-based RITDs and HEMTs have the potential to set new standards for high speed and low-power consumption. NRL is developing the building blocks needed to build digital circuits in the antimonide-based system. We plan to monolithically integrate AlSb/InAs/GaSb RITDs and AlSb/InAs HEMTs to form logic circuits. These circuits will utilize the monostable-bistable transition logic element (MOBILE),[18] which is a basic building block of various logic circuits. The HEMT performs optimally at a very low drain voltage (see Figure 7) which makes it the preferred choice to efficiently exploit the low-voltage, low-power performance advantages of AlSb/InAs/GaSb RITDs (see Figure 9). These RITDs are expected to operate at speeds in excess of 100 GHz. Both the antimonide-based RITD, with the peak current occurring near 100 mV, and the antimonide-based HEMT work well at voltages less than 500 mV. This low-voltage operation leads to the prospect of very low power dissipation in the MOBILE configuration. The integration of the RITD and the HEMT is a critical advancement which will provide the enabling technology needed for a new class of very dense, ultra-high-speed logic circuits with high functionality and very low power dissipation.

4. MID-WAVE IR LASERS

For semiconductor diode lasers in the visible and near IR wavelengths, there is an established and relatively mature technology. However, at mid-IR wavelengths (3-10 μm), the development of analogous devices with non-cryogenic operating temperatures and high output powers has proven to be much more challenging. Infrared countermeasure programs of the Navy/Marine Corps need high power mid-IR sources. Mid-IR sources are also needed in chemical sensing applications that detect conventional, chemical and biological weapons as well as commercial applications. We are engaged in developing a new mid-IR laser source based on type-II InAs/InGaSb/AlSb multiple quantum wells.[19] An energy diagram showing the heterostructure is indicated in Figure 10. The laser consists of several tens of periods of the active unit, a four-constituent quantum well (InAs-InGaSb-InAs-AlSb). The AlSb barriers preserve the two-dimensional dispersion relations for both electrons and holes, and as a result, yield a larger optical matrix element than that of InAs-InGaSb superlattices. In addition, the flexibility offered by band structure engineering allows the deleterious impact of non-radiative Auger recombination to be minimized. The lasing transition is between electrons mainly localized in the InAs layers with holes localized in the InGaSb.

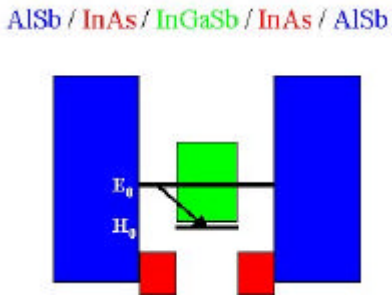

Figure 10 — Heterostructure energy diagram for the optically pumped mid-IR laser.

We have optimized the growth for infrared laser structures by addressing three important growth issues: the optimum growth temperature, the interfacial bond type, and the antimony source. More than two dozen multiple quantum well samples with 20 periods have been grown with a systematic variation of the growth parameters. Each quantum well consists of four constituent layers, InAs/InGaSb/InAs/AlSb, and their thicknesses are 5-5.5/10/5-5.5/14 MLs, respectively. The layer thickness was calibrated during the GaSb and AlSb buffer growth and monitored during the quantum well growth by RHEED oscillations. Because there is not a common cation nor anion between adjacent layers, it is possible to have different interfacial bond

types between layers depending on the shutter sequence (see Figure 2). For example, either InSb-like or GaAs-like interfaces can be formed between InAs and InGaSb layers. In addition, with both cracked and uncracked Sb cells available in our MBE system, laser samples grown using dimer Sb_2 or tetramer Sb_4 source can be studied.

A series of reference samples were grown on GaSb substrates at different growth temperatures using Sb_2. A shutter sequence yielding InSb-like interfacial bonds was used. For example, after 10 MLs of InGaSb, the surface is soaked with Sb for 2 s, followed by 1 ML of In. Subsequently, 4 ML of InAs is grown, followed by 1 ML of In and then 2 s of Sb. The total InAs layer thickness is 5 ML including half an interfacial bond on each side. All samples were examined and investigated by Nomarski phase-contrast optical microscopy, single- or double-crystal X-ray diffraction and variable temperature PL.[20] The optimum growth temperature[21] is found to be 420 ± 20ºC, which is centered 10ºC below the (1x5) to (1x3) RHEED phase transition temperature of GaSb under a V/III flux ratio of two. Away from this optimum growth temperature range, the samples have poorer surface morphology, broader X-ray peaks, and lower PL intensity.

In order to compare the impact of different interfacial bond types, two samples were grown with GaAs and AlAs-like interfaces within the optimum growth temperature range. The samples show good surface morphology with low defect density, and excellent x-ray diffraction patterns. However, the PL intensity is one order of magnitude lower over the temperature ranging from 4K to 300K. This finding implies that although superior structural properties can be maintained, the GaAs interfaces are deleterious to the optical performance. This degradation is probably due to the formation of non-radiative recombination centers at interfaces. Other workers have previously reported greatly reduced mobilities and increased carrier concentrations for InAs/AlSb FET structures produced with AlAs-like interfacial bonds.[22] Presumably the formation of electrically-active and non-radiative defect sites during the growth of the GaAs/AlAs-like interface is the cause of the degradation of both the laser and FET performance. We have also grown two samples identical to the reference samples with InSb bond type within the optimum growth temperature using uncracked Sb_4. Both Nomarski microscopy and X-ray diffraction indicate inferior structural properties for samples grown with an uncracked Sb source. The PL of these two samples is just slightly lower than that of reference samples at room temperature. Unlike the monotonic increase of PL intensity with decreasing PL measurement temperature for the reference samples, the PL intensity first increases from 300K to ~50K, and then exhibits steep reduction down to 4K. This observation suggests additional trap states introduced by an uncracked Sb source.

With the knowledge we gained from the growth study, we grew two complete laser structures with InSb-like interfacial bonds using the cracked Sb source at the optimum growth temperature. The samples comprise 50 periods of active quantum wells, sandwiched between 2.5 μm-thick AlSb on each side to confine the optical wave. The thicknesses of each layer are 5.5/8.5/5.5/14 ML with $In_{0.26}Ga_{0.74}Sb$. The samples were fabricated into ridge laser structures and optically pumped with a 2.1 μm Ho:YAG laser. The results from this study are shown in Figure 11. The peak output power at 4.1 μm exceeded 1.5 W/facet at 300 K,[23] about ten times higher than any previously published result at this wavelength at the time. Recently we have extended our laser studies to longer wavelength. In this work, lasers have been fabricated that operate continuous wave (CW) from 5.9-7.1 μm at temperatures between 210-130 K, respectively.[24] Although these CW lasers would still require cryogenic cooling, they produced CW output powers of 70-30 mW for lasers with wavelengths between 4.2-6.1 μm at 78 K, respectively. This **CW** result at 6.1μm exceeds the previous maximum wavelength of 5.3 μm for any **pulsed** III-V interband semiconductor laser.

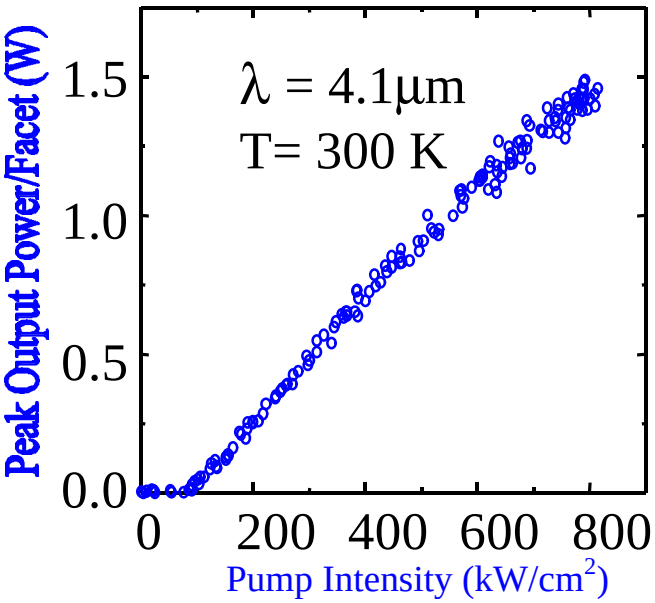

Figure 11—Room temperature operation of a pulsed, optical pumped InAs/InGaSb/AlSb mid-IR laser.

5. FAR-IR DETECTORS

The theoretically predicted intrinsic material properties of superlattices constructed from InGaSb/InAs suggest it is possible to construct multi-color long-wavelength IR (LWIR) focal plane arrays an order of magnitude more sensitive than those based on HgCdTe.[25] This flexibility in wavelength control comes from the type II band alignment between InAs and InGaSb denoted in Figure 12. By changing the layer thicknesses of InGaSb and InAs it is possible to vary the energy of the conduction band edge, E_0, and valence band edge, H_0, of the superlattice and tune the energy gap, $E_{gap}=E_0-H_0$, from nearly zero to 0.5 eV. Although the initial results obtained from these devices are promising, the existence of poorly understood Shockley-Read recombination centers and high reverse-bias leakage currents limit the ultimate device performance. We are engaged in a focussed effort to determine whether or not these limitations can be overcome and a new generation of high-sensitivity, high-temperature, multi-color, LWIR detectors can be developed.

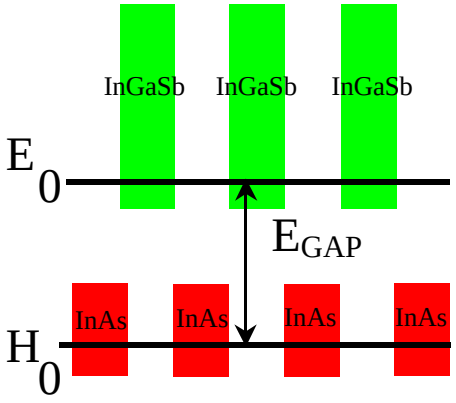

Figure 12—Energy level diagram for an InAs/InGaSb superlattice.

NRL is involved in the MBE growth of detector structures, the fabrication of detector elements, and the measurement of detector efficiency. We are examining how changes in the growth and processing procedures impact the concentration and type of Shockley-Read centers and reverse-bias leakage currents. In particular, we are investigating the role of interface formation (including growth interrupts), growth temperature, strain, and anion species (e.g. Sb_4 vs. Sb_2 vs. Sb_1). RHEED, x-ray diffraction, STM, PL, and TEM are used to evaluate growth procedures. The improved growth procedures will be incorporated into LWIR device structures to determine the impact on detector performance. If this program is successful, InAs/InGaSb superlattice detectors could replace HgCdTe in long-wavelength, high-performance infrared applications where operating temperature is a critical parameter.

In order to obtain large absorption from an InAs/InGaSb superlattice an epitaxial film with a thickness of several microns is required. However, if a good lattice match between the substrate and the epifilm is not maintained during MBE growth, dislocations will form in the epilayer. These dislocations are expected to result in an increase in leakage currents in p-i-n diodes and thereby degrade detector performance. A superlattice with 13 ML InAs and 8 ML $In_{0.15}Ga_{0.85}Sb$ was designed to have a cut-off wavelength of 10 μm. If interface bonds are neglected, an unrealistic assumption, the average lattice constant of this structure is calculated to be 6.094 Å, an excellent match with a GaSb substrate (6.095 Å). If InSb interface bonds are included, the lattice constant increases to 6.112 Å; for GaAs bonds, the average lattice constant is 6.074 Å. In both cases, the magnitude of the lattice mismatch with GaSb is 0.3%. A mismatch of this size could result in the formation of misfit dislocations for the 1-3 μm-thick SLs required for high absorption in IR detectors. In order to get a good lattice match with the GaSb substrate, a structure with alternating interface bond type was chosen. The GaAs bonds are used for the transition from InAs to InGaSb; InSb bonds are used for the InGaSb-to-InAs interface. In this way, layers of InGaSb are never exposed to an As flux, a procedure that our previous work indicated caused significant intermixing.

A series of 100-period superlattices was grown with the above structure. The substrate temperature was varied from 350-420 ^oC. Layer thicknesses were confirmed by measuring RHEED oscillations during the SL growth. In all cases, x-ray diffraction measurements revealed superlattices lattice-matched to GaSb within 0.1%. The intensity and widths of the x-ray SL satellites were superior for growth temperatures of 380-420 ^oC. Optical microscopy measurements revealed increasing defect densities with increasing temperature in this range. For this reason, 380^oC was chosen as the growth temperature for p-i-n structures. Photoluminescence measurements confirmed a band-gap near 10 μm. Fabrication and testing of p-i-n detectors is in progress at NRL.

The best detector characteristics reported to date are from the recent work of Fuchs and coworkers at the Fraunhofer Institute.[26] They used MBE to fabricate InAs/InGaSb homojunction p-i-n detectors. For 8 μm photodiodes the Johnson-noise-limited detectivity at 77 K was $D^*\sim10^{12}$ $cmHz^{1/2}/W$. While this sensitivity is still less than one can obtain from HgCdTe, additional work is expected to lead to improvements that may ultimately allow the InAs/InGaSb detectors to exhibit superior performance.

6. SUMMARY

Heterostructures formed from the 6.1 Å family of III-V semiconductors allow materials properties to be engineered with enormous flexibility. The combination of this flexibility with the improvements in material quality has allowed the demonstration of high-speed, low-power FETs and RITDs, mid-IR lasers and long-wavelength IR detectors. Based on intrinsic advantages obtained from band-structure engineering, these electronic and optoelectronic devices hold the promise to define a new state of the art in performance that can not be met by competing technologies. In the next decade additional improvements in materials quality and device design should allow this promise to be realized.

7. ACKNOWLEDGMENTS

The Office of Naval Research, the Air Force Research Laboratory and DARPA supported this work.

8. REFERENCES

1. I. H. Campbell, I. Sela, B. K. Laurich, D. L. Smith, C. R. Bolognesi, L. A. Samoska, A. C. Gossard and H. Kroemer, "Far-Infrared Photoresponse of the InAs/GaInSb superlattice", Appl. Phys. Lett. 59 846 (1991).
2. T. C. Hasenberg, D. H. Chow, A. R. Kost, R. H. Miles and L. West, "Demonstration of 3.6μm $Ga_{1-x}In_xSb$/InAs Superlattice Diode Laser", Electron. Lett. 31 275 (1995).
3. J. D. Werking, C. R. Bolognesi, L. D. Chang, C. Nguyen, E. L. Hu and H. Kroemer, "High-Transconductance InAs/AlSb Heterojunction Field-Effect Transistors with δ-Doped AlSb Upper Barriers", IEEE Electron Device Lett. 13 164 (1992).
4. J. R. Soderstrom, D. H. Chow and T. C. McGill, "New Negative Differential Resistance Device Based on Resonant Interband Tunneling", Appl. Phys. Lett. 55 1094 (1989).
5. D. Gammon, B. V. Shanabrook and D. S. Katzer, "Excitons, Phonons, and Interfaces in GaAs/AlAs Quantum Well Structures", Phys. Rev. Letters 67 1547 (1991).
6. Brian R. Bennett, B. V. Shanabrook, R. J. Wagner, John L. Davis and James R. Waterman, "Control of Interface Stoichiometry in InAs/GaSb Superlattices Grown by Molecular Beam Epitaxy", Appl. Phys. Lett. 63 949 (1993) and references therein.
7. Brian R. Bennett, B. V. Shanabrook and E. R. Glaser, "Interface Control in InAs/AlSb Superlattices", Appl. Phys. Lett. 65 598 (1994).
8. B. V. Shanabrook and B. R. Bennett, "Planar Vibrational Modes as Probes of Interface Structure", Phys. Rev. B 50 1695 (1994) and references therein.
9. P. M. Thibado, B. R. Bennett, M. E. Twigg, B. V. Shanabrook and L. J. Whitman, "Origins of Interfacial Disorder in GaSb/InAs Superlattices", Appl. Phys. Lett., 67 3578 (1995), P. M. Thibado, B. R. Bennett, B. V. Shanabrook and L. J. Whitman, "A RHEED and STM Study of Sb-rich GaSb and AlSb (001) Surface Reconstruction", J. Cryst. Growth, 175 317 (1997) and L. J. Whitman, P. M. Thibado, S. C. Erwin, B. R. Bennett and B. V. Shanabrook, "Metallic III-V (001) surfaces: Violations of the Electron Counting Model", Phys. Rev. Lett. 79 693 (1997).
10. M.E. Twigg, B. R. Bennett, P. M. Thibado, B. V. Shanabrook and L. J. Whitman, "Interfacial Roughness in InAs/GaSb Superlattices Grown by MBE", Phil. Mag. A 77 7 (1998) and references therein.
11. B. Z. Nosho, W. H. Weinberg, W. Barvosa-Carter, B. R. Bennett, B. V. Shanabrook, and L. J. Whitman, "Effects of Surface Reconstruction on III–V Semiconductor Interface Formation: The Role of III/V Composition", Appl. Phys. Lett. 74 1704 (1999) and references therein.
12. J. B. Boos, W. Kruppa, B. R. Bennett, D. Park, S. Kirchoefer, R. Bass, and H. B. Dietrich, "AlSb/InAs HEMTs for Low-Voltage, High-Speed Applications", IEEE Trans. on Electron Devices 45, 1869 (1998) and J. B. Boos, B. R. Bennett, W. Kruppa, D. Park, M. J. Yang, and B. V. Shanabrook, "AlSb/InAs HEMTs Using Modulation InAs(Si) Doping", Electron. Lett. 34, 403 (1998).
13. B. R. Bennett, M. J. Yang, B. V. Shanabrook, J. B. Boos and D. Park, "Modulation Doping of InAs/AlSb Quantum Wells Using Remote InAs Donor Layers", Appl. Phys. Lett. 72 1193 (1998).
14. J. B. Boos, M. J. Yang, B. R. Bennett, D. Park, W. Kruppa, C. H. Yang, and R. Bass, "0.1 μm AlSb/InAs HEMTs with an InAs Subchannel", Electron. Lett. 34, 1525 (1998).
15. J. B. Boos, B. R. Bennett, W. Kruppa, D. Park, J. Mittereder, R. Bass, and M. E. Twigg, "Ohmic Contacts in AlSb/InAs High Electron Mobility Transistors for Low-Voltage Operation", J. Vac. Sci. Technol. B 17(3), May/June 1999.
16. E. R. Brown, J. R. Soderstrom, C. D. Parker, L. J. Mahoney, K. M. Molvar and T. C. McGill, "Oscillations up to 712 GHz in InAs/AlSb Resonant Tunneling Diodes", Appl. Phys. Lett. 58, 2291 (1991).

17. B. Z. Nosho, W. H. Weinberg, W. Barvosa-Carter, A. S. Bracker, R. Magno, B. R. Bennett, J. C. Culbertson, B. V. Shanabrook and L. J. Whitman, to be published in J. Vac. Sci. Technol. B (1999).
18. K. Maezawa and Takashi Mizutani, "A New Resonant Tunneling Logic Gate Employing Monostable-Bistable Transition", Jpn. J. Appl. Phys. 32, L42 (1993).
19. J. R. Meyer, C. A. Hoffman, F. J. Bartoli, and L. R. Ram-Mohan, "Type-II Quantum-Well Lasers for the Mid-Wavelength Infrared", Appl. Phys. Lett. 67, 757 (1995) and J. R. Meyer, C. A. Hoffman, and F. J. Bartoli, Patent # 5,793,787, August 11, 1998, "Type-II Quantum-Well Laser with Enhanced Optical Matrix Elements." (Navy Case # 77,044, Patent Application Serial # 08/585,612)
20. M. J. Yang, W. J. Moore, B. R. Bennett, B. V. Shanabrook, J. O. Cross, W. W. Bewley, C. L. Felix, I. Vurgaftman, and J. R. Meyer, "Optimum Growth Parameters for Type-II Infrared Lasers," to be published in J. Appl. Phys., (1999).
21. M. J. Yang, W. J. Moore, C. H. Yang, R. A. Wilson, B. R. Bennett, B. V. Shanabrook, "Determination of Temperature Dependence of GaSb Absorption Edge and its Application for Transmission Thermometry," to be published in J. Appl. Phys. (1999).
22. G. Tuttle, H. Kroemer and J. H. English, "Effects of Interface Layer Sequencing on the Transport Properties of InAs/AlSb Quantum Wells: Evidence for Antisite Donors at the InAs/AlSb Interface", J. Appl. Phys. 67 3032 (1990).
23. W. W. Bewley, C. L. Felix, E. H. Aifer, I. Vurgaftman, L. J. Olafsen, J. R. Meyer, H. Lee, R. U. Martinelli, J. C. Connolly, A. R. Sugg, G. H. Olsen, M. J. Yang, B. R. Bennett and B. V. Shanabrook, "Above-Room-Temperature Optically Pumped Midinfrared W Lasers", Appl. Phys. Lett. 73 3833 (1998).
24. W. W. Bewley, C. L. Felix, I. Vurgaftman, D. W. Stokes, E. H. Aifer, L. J. Olafsen, J. R. Meyer, M. J. Yang, B. V. Shanabrook, H. Lee, R. U. Martinelli and A. R. Sugg, "High-Temperature Continuous-Wave 3–6.1 μm "W" Lasers With Diamond-Pressure-Bond Heat Sinking", Appl. Phys. Lett. 74 1075 (1999).
25. C. H. Grein and H. Ehrenreich, "Improvement of Infrared Detector Performance in Carrier Depleted Strained Layer Type II Superlattices", J. Appl. Phys. 82 6365 (1997) and references therein.
26. F. Fuchs, U. Weimer, W. Pletschen, J. Schmitz, E. Ahlswede, M. Walther, J. Wagner, and P. Koidl, "High Performance InAs/$Ga_{1-x}In_xSb$ Superlattice Infrared Photodiodes", Appl. Phys. Lett. 71 3251 (1997).